J Mater Sci (2013) 48:8259–8267
DOI 10.1007/s10853-013-7638-5

First principles study of electronic and optical properties of Cu_2ZnSnX_4 (X = S, Se) solar absorbers by Tran–Blaha-modified Becke–Johnson potential approach

Anima Ghosh · R. Thangavel · M. Rajagopalan

Received: 22 May 2013 / Accepted: 29 July 2013 / Published online: 9 August 2013

Abstract The electronic and optical properties of Cu_2ZnSnX_4 (X = S, Se) have been studied using the highly accurate Tran–Blaha-modified Beck and Johnson (TB-mBJ) potential. From this study, it has been found that these compounds are direct band semiconductors and the value of band gap increases from Se to S. The values of the band gap, density of states, bulk modulus, dielectric functions, real part of optical conductivity, and absorption coefficient are reported. The calculated band gap value is found to be in excellent agreement with the recent experimental results. A comparison of the calculated properties with available experimental data indicates that the TB-mBJ approach provides a better description of the electronic and optical properties of the compound than the standard GGA approaches.

Introduction

Copper–zinc–tin–chalcogenides-based quaternary semiconductors have received wide attention as potential solar cell absorber materials. An ideal solar energy absorber should have a band gap around 1.5 eV and a high optical absorption coefficient for the visible light. Based on this fact, the band gaps and optical properties of the copper-based systems were extensively studied both experimentally [1–3] and theoretically [4, 5]. The band gap energy (E_g) of Cu_2ZnSnS_4 (CZTS) and $Cu_2ZnSnSe_4$ (CZTSe) are around 1.0–1.5 eV, which is suitable for photovoltaic applications. Moreover, knowledge of the optical properties, such as the dielectric function and the optical absorption coefficient, is required to analyse optical measurements as well as to optimize the solar cell devices. Various research groups reported the electronic structure calculations [4–8]. But new approach, such as TB-mBJ, is introduced recently. Overall, TB-mBJ is a decent alternative for GW or hybrid functional, achieving a comparable accuracy at a far lower cost. The combination of TB-mBJ exchange and generalise gradient approximation (GGA) correlation produced accurate semiconductor gaps for numerous semiconductors and insulators [9–13]. In this paper, the full potential linearized augmented plane wave (FP-LAPW) method with the TB-mBJ potential has been used to investigate the electronic and optical properties of the copper-based solar cell materials.

A. Ghosh · R. Thangavel (✉)
Department of Applied Physics, Indian School of Mines, Dhanbad 826004, Jharkand, India
e-mail: rthangavel@gmail.com; thangavel.r.ap@ismdhanbad.ac.in

M. Rajagopalan
Crystal Growth Centre, Anna University, Chennai 600025, India

Method of calculation

As a computational tool, for Cu_2ZnSnX_4 (X = S, Se), we have employed the full potential augmented plane wave method (APW + lo) based on density functional theory (DFT) using Vienna package WIEN2K code (FP-LAPW) [14]. We have used the GGA within the Perdew–Burk–Ezrenhof (PBE) parameterization [15] and TB-mBJ [9–11] potential. A plane wave expansion has been done with $K_{max} \times R_{max}$ equal to 7 and $l_{max} = 10$ are kept constant throughout the calculations. The charge density is Fourier expanded up to $G_{max} = 12(Ry)^{1/2}$. A 2 × 2 × 2 division for k-point sampling is used, and the tetrahedral method [16] has been employed for the Brillouin zone integrations. The Zn ($3d^{10}$ $4s^2$), Cu ($3p^6$ $4s^2$ $3d^9$), Sn ($4d^{10}$ $5s^2$ $5p^2$),

S ($3s^2$ $3p^4$), and Se ($3d^{10}$ $4s^2$ $4p^4$) orbital are treated as valence states. The muffin tin radii for Zn, Cu, Sn, S, and Se are chosen to be 2.25, 2.22, 2.48, 1.97, and 1.97 a.u., respectively, for stannite structure and for kesterite structure, the radii are 2.22, 2.34, 2.41, 1.91, and 1.91 a.u., respectively. A number of iterations (40) are dedicated to accomplish self consistency. Less than 0.00001Ry of the total energy difference is used as per formula unit for succeeding iterations.

The frequency-dependent complex dielectric function $\varepsilon(\omega) = \varepsilon_1(\omega) + i\varepsilon_2(\omega)$ is known to describe the optical response of the medium at all phonon energies $E = \hbar\omega$. The imaginary part of the $\varepsilon_2(\omega)$ in the long wavelength limit has been obtained directly from the electronic structure calculation, using the relation [17],

$$\varepsilon_2(\omega) = \left(\frac{4\pi^2 e^2}{m^2\omega^2}\right)\sum_{i,j}\int \langle i|M|j\rangle^2 f_i(1-f_i)\delta(E_f - E_i - \omega)d^3k, \tag{1}$$

where M is the dipole matrix, i and j are the initial and final states, respectively, f_i is the Fermi distribution function for the ith state, and E_i is the energy of electron in the ith state. The real part of the dielectric function $[\varepsilon_1(\omega)]$ can be extracted using the Kramers–Kronig relation [18]

$$\varepsilon_1(\omega) = 1 + \frac{2}{\pi}p\int_0^\infty \frac{\omega'\varepsilon_2(\omega')d\omega'}{\omega'^2 - \omega^2}, \tag{2}$$

where p stands for the principal value of the integral. The knowledge of both the real and imaginary parts of the dielectric tensor allows the calculation of the important optical properties, such as absorption coefficient, electron energy loss function, and real part of optical conductivity.

The absorption coefficient, $\alpha(\omega)$ and real part of the optical conductivity, $\mathrm{Re}[\sigma(\omega)]$ are calculated using the relation as follows [19–21]:

$$\alpha(\omega) = \sqrt{2}\omega\left[\sqrt{\varepsilon_1^2(\omega) + \varepsilon_2^2(\omega)} - \varepsilon_1(\omega)\right]^{1/2}, \tag{3}$$

$$\mathrm{Re}[\sigma(\omega)] = \frac{\omega\varepsilon_2}{4\pi}. \tag{4}$$

Results and discussion

Structural properties

The crystalline and optical properties of CZTS and CZTSe have been discussed and compared with available literature results [1, 5]. The I_2–II–IV–VI_4 quaternary semiconductors have two fundamental crystal structures: one is the kesterite structure (KS) [space group $I\bar{4}$], the other is the stannite structure (SS) [space group $I\bar{4}2m$], which are shown in Fig. 1. In all of the structures, Se or S (group VI) atom is surrounded by two Cu (group I) atoms, one Sn (group IV) atom and one Zn (group II) atom, therefore, the octet rule is obeyed.

The calculated total energies within GGA as function of the volume were used for determination of theoretical lattice constant and bulk modulus. Equilibrium lattice constant, bulk modulus and its pressure derivative are calculated by fitting the calculated total energy to the Murnaghan's equation of state given in equation

$$E(V) = E_0 + \left[\frac{(V_0/V)^{B_0'}}{B_0' - 1} + 1\right] - \frac{B_0 V_0}{B_0' - 1}, \tag{5}$$

where E_0 is the minimum energy at $T = 0$ K, B_0 is the bulk modulus at the equilibrium volume, and B_0' is pressure derivative of the bulk modulus at the equilibrium volume. The equilibrium volume is given by the corresponding total energy minimum as shown in Fig. 2a–d. The volume corresponding to the lowest energy is used in the determination of equilibrium lattice constant. The calculated values of lattice constant and bulk modulus are presented in Table 1. It is clearly seen that the structural stability of these compounds is more stable in kesterite than stannite structure. We have also optimized the positional parameter and the c/a ratio for all the compounds; it is found that the c/a ratio is very close to 2. The bulk modulus is slightly higher in KS when compared to SS for CZTS; whereas the bulk modulus is greater in SS when compared to KS for CZTSe. The calculated lattice constants for both KS and SS are in good agreement with the experimental values.

Density of states (DOS)

Figure 3a–d shows calculated partial and total density of states for all four CZTS and CZTSe. Overall, they have rather similar energy distribution of the eigenstates. The VB–DOS contains mainly a hybridization of Cu-d and

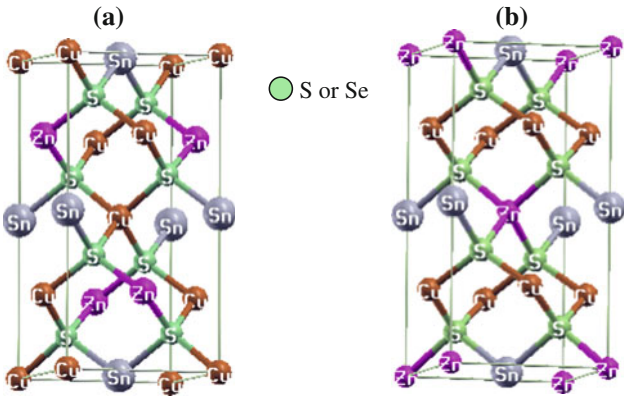

Fig. 1 (Color online) The crystal structures of CZTS_KS and CZTS_SS, respectively

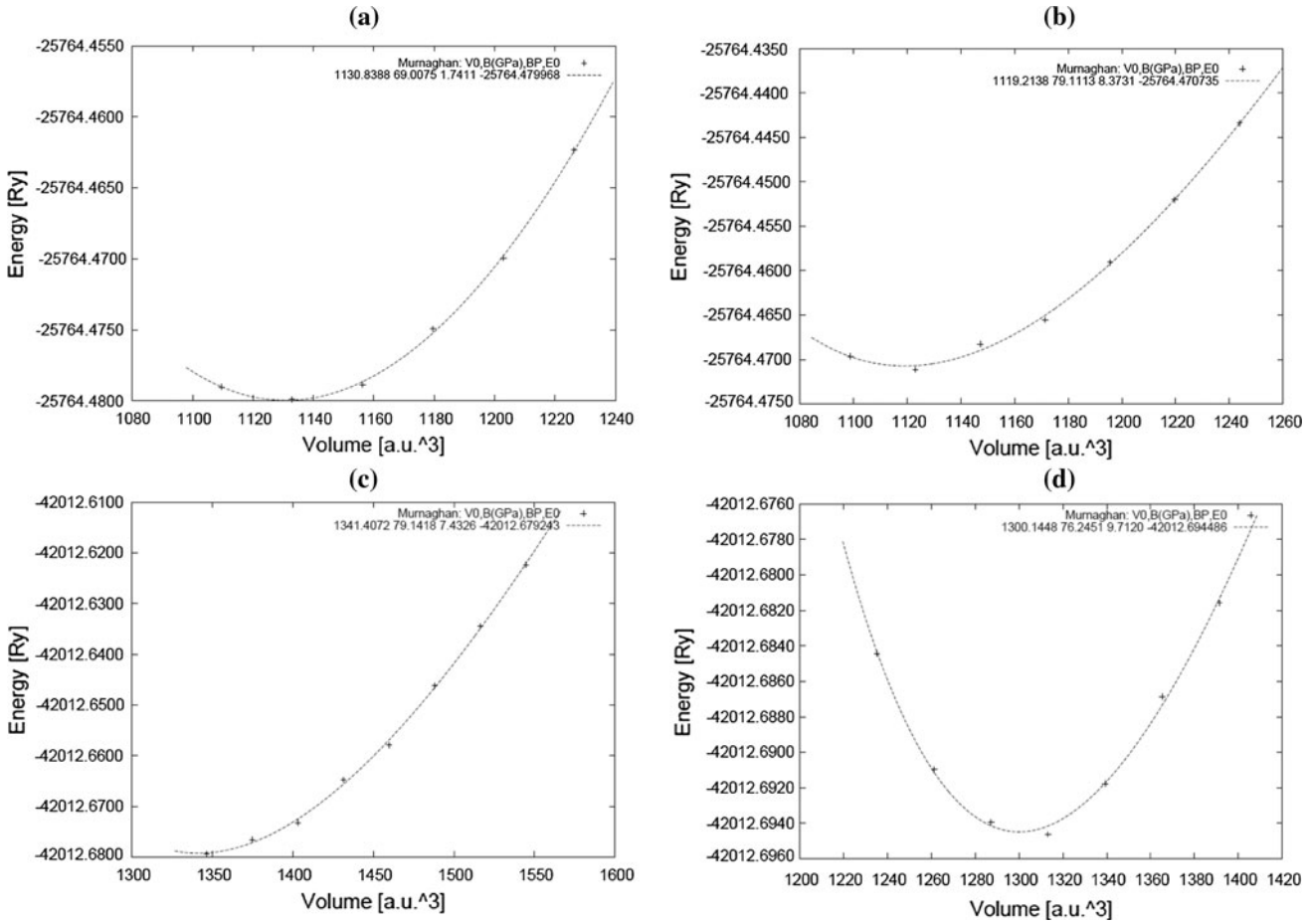

Fig. 2 (Color online) **a–d** represent the equilibrium volume with corresponding total energy minimum of CZTS_KS, CZTS_SS, CZTSe_KS, and CZTSe_SS, respectively

Table 1 Structural properties of tetragonal body-centered structure: equilibrium lattice parameter (a.u.), c/a ratio, and anion position are given in fractions of the lattice vectors, bulk modulus (GPa), GGA band gap (eV), and TB-mBJ band gap (eV)

Component	Lattice parameter, a (Å)	c/a ratio	Anion position (X, Y, Z)	Bulk modulus (GPa)	Band gap (eV)	
					GGA	TB-mBJ
CZTS_KS	5.574, 5.428[a], 5.432[c]	1.996, 1.996[c]	0.756, 0.764, 0.871	80.9, 86.8[d]	0.98	1.18, 1.48[b], 1.5[e]
CZTS_SS	5.637, 5.434[a], 5.462[f]	1.996, 1.992[f]	0.757, 0.757, 0.866	77.3, 86.9[d]	0.93	1.17, 1.45[f]
CZTSe_KS	5.941, 5.687[a], 5.680[h]	2.000, 2.000[h]	0.757, 0.757, 0.870	77.39	1.04	1.23, 1.44[g]
CZTSe_SS	5.676, 5.688[a], 5.684[i]	1.999, 1.997[i]	0.757, 0.757, 0.866	77.75	0.86	1.11, 0.9[i]

[a] Reference [1]
[b] Reference [22]
[c] Reference [34]
[d] Reference [35]
[e] Reference [24]
[f] Reference [25]
[g] Reference [23]
[h] Reference [36]
[i] Reference [26]

anion (S and Se)-*p*, although there are also contributions from Zn-*spd*, Cu-*s*, and Sn-*p* in the lower energy region of the DOS (i.e., −6.5 to −2 eV). The CB-DOS consists mainly of cation-*s* anion-*p* hybridization. In the range between −2.5 and −4 eV below the Fermi level, Sn-*p* shows highest contribution. Within the range −1.28 to 1.5 eV around E_F, Zn-*s* shows major contribution. On the other hand, in conduction band side anion, (S and Se)-*p* shows a peak in between 1.2 and 1.7 eV. So, the band gap is formed between the hybridized "*p*" like states of anion in the valence band and the antibonding states in the conduction band of Zn-*s* like states [1, 21].

By analyzing the partial density of these compounds, it is found that the *s*–*p* interaction modifies the gap of these materials. The anion-*p* like states are pushed up and Zn-*s* like states are pushed down. The bands above 2.5 eV mainly consists of the hybridised bands of Zn "*s*" like, Sn "*p*" like and anion "*p*" like bands. The energy gap is about 1.5 eV. The higher CBs do not contribute to the optical absorption in the low-energy regime. The calculated band gap values are reported in Table 1. Moreover, our calculated band gap values are in good agreement with earlier theoretical predictions and experimental investigations [1, 22–26].

Optical properties

The optical properties of the CZTX (X = S, Se) can be described by means of complex dielectric function $\varepsilon(\omega)$. The dielectric function describes the linear response of the system to an electromagnetic radiation, which is related to the interaction of photons with the electrons. The magnitude of optical properties depends on the polarization of photons. For the tetragonal unit cell structure, we calculate

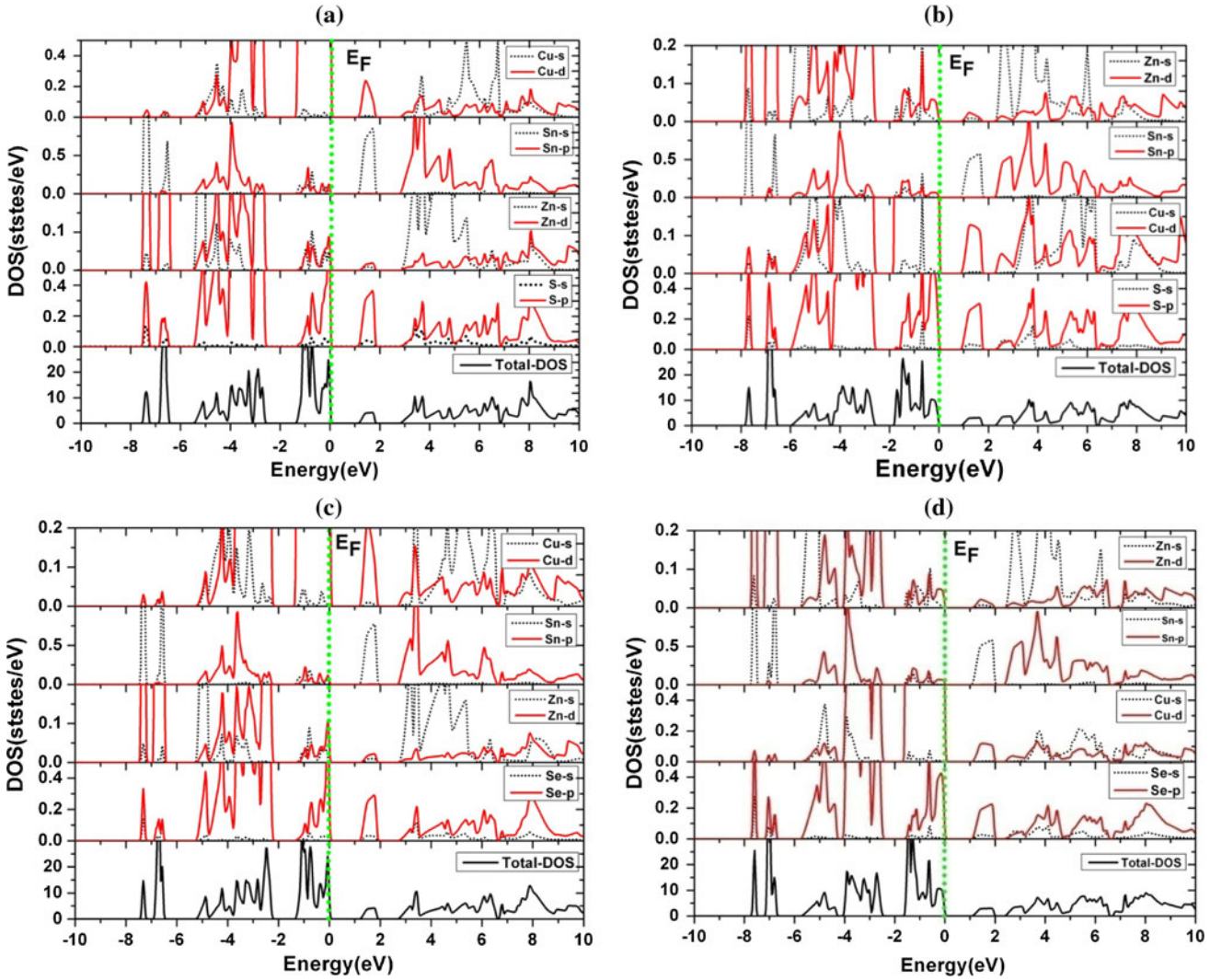

Fig. 3 (Color online) **a–d** represent the calculated partial density of states and total density of states with the TB-mBJ approximation for CZTS_KS, CZTS_SS, CZTSe_KS, and CZTSe_SS, respectively

two independent components of dielectric constant $\varepsilon(\omega)$. One perpendicular component and the other parallel component, which arises due to polarization along the z direction. All the other optical constants, such as refractive index $n(\omega)$, the extinction coefficient $k(\omega)$, the optical reflectivity $r(\omega)$, and absorption coefficient $\alpha(\omega)$, are then computed from the components of the dielectric function.

Figures 4 and 5a–d show the real and imaginary parts of the dielectric function. The real part of the dielectric function, $\varepsilon_1(\omega)$, represents the dispersion of the incident photons by the materials, while imaginary part of the dielectric function, $\varepsilon_2(\omega)$ is related to the energy absorbed by the material. The values of the static dielectric constant for a field perpendicular or parallel to the tetragonal c-axis are listed in Table 2. The dielectric constant $\varepsilon_1(0)$ is obtained from the zero-frequency limit of $\varepsilon_1(\omega)$ and it corresponds to the electronic part of the static dielectric constant of the material. It is a parameter of fundamental importance in many aspects of materials properties.

From the application point of view, it is very interesting to determine the transition corresponding to each peak in the spectrum. The peak in the $\varepsilon_2(\omega)$ spectrum distributes in a sequence similar to that in density of states. The main difference of dielectric functions between TB-mBJ and GGA becomes noticeable in the energy range from 0 to 5 eV. Transitions from valence bands at top to conduction bands at the lower state contribute to the optical spectra's major part [21]. The dramatically increasing point of the mBJ imaginary part ε_2 is shifted to higher photon energy with respect to that of the GGA ε_2. The rightward shift of the TB-mBJ ε_2 results between 2 and 5 eV with respect to the GGA ones reflects the fact that the TB-mBJ energy gap

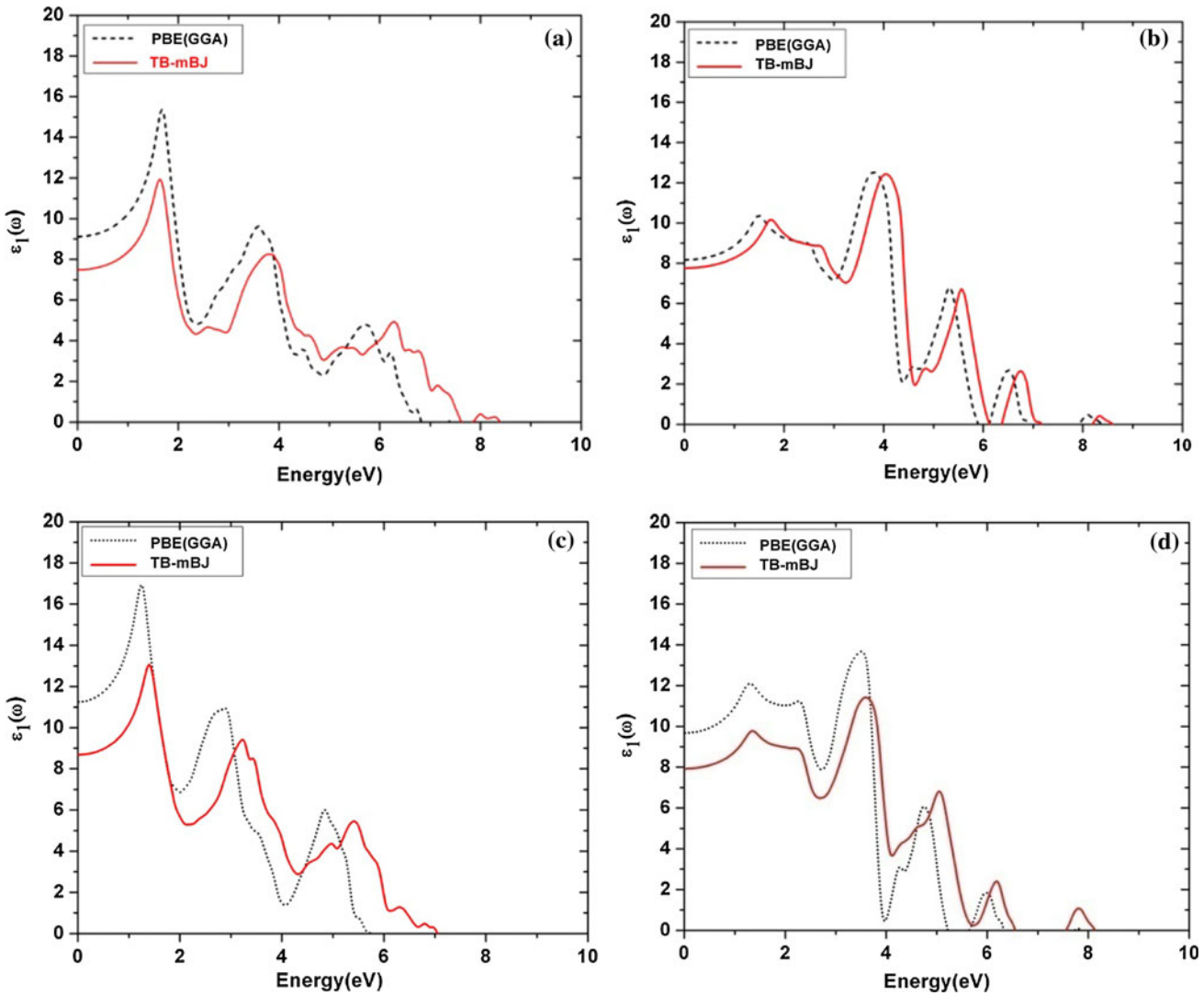

Fig. 4 (Color online) **a–d** represent the real (ε_1) parts of dielectric functions versus photon energy (eV). *Solid lines* show the TB-mBJ results, and *dashed lines* the GGA ones

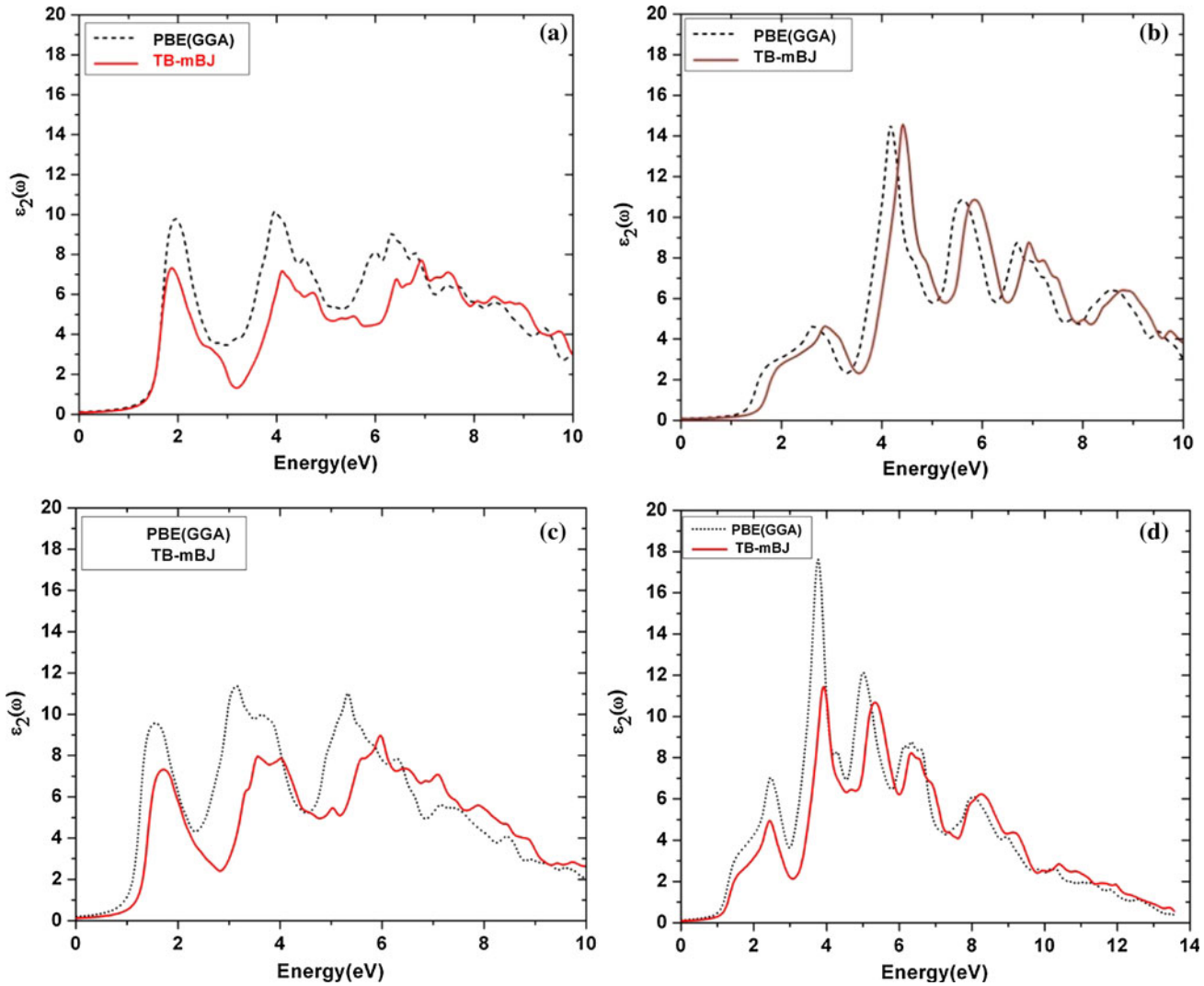

Fig. 5 (Color online) **a–d** represent the imaginary (ε_2) parts of dielectric functions versus photon energy (eV) for CZTS_KS, CZTS_SS, CZTSe_KS, and CZTSe_SS, respectively. *Solid lines* show the TB-mBJ results, and *dashed lines* the GGA ones

Table 2 Scissor correction in eV and real part of dielectric functions $\varepsilon_0(\omega)$ at zero frequency using both PBE (GGA) and TB-mBJ potentials

Components	Energy shift (scissor correction)		$\varepsilon_0(\omega)$	
	GGA	TB-mBJ	GGA	TB-mBJ
CZTS_KS	0.51	0.32	9.09	7.44, 6.8[a], 6.79[b]
CZTS_SS	0.57	0.33	8.09	7.72, 6.5[a], 6.53[b]
CZTSe_KS	0.0	0.00	11.26	11.26, 8.6[a], 8.00[b]
CZTSe_SS	0.14	0.00	9.64	9.64, 8.2[a], 8.18[b]

[a] Reference [1]

[b] Reference [3]

is substantially improved over the GGA one. The zero-frequency real part ε_1 of static dielectric functions and scissor operator are reported in Table 2, in comparison with earlier calculated value [1, 5, 27].

Furthermore, the dielectric functions of all four components have a strong $\varepsilon_2(\omega)$ peak in the energy range between 3.6 and 4.3 eV. This peak arises from the response at $\overrightarrow{k}$-states always from the Γ-point, with a strong contribution from the flat dispersion of the top most VB and of the lowest CB. The two kesterite compounds have more pronounced peaks around 1.6–2.0 eV, whereas the two stannite compounds show much stronger anisotropy of their response peaks. In the kesterite compounds, the upper VBs are energetically close together at 0–0.5 eV at the BZ edges, whereas the upper VBs in the stannite compounds have more split with energy in the region of about 0.5–1.0 eV. It is the symmetry of these VBs in combination with their energy dispersions that cause the anisotropy [1, 5].

The calculated real part of the optical conductivity (frequency dependent) using GGA and TB-mBJ potentials is shown in Fig. 6a–d. The material's conductivity

increases with an increase of energy from 3.3 to 9.03 eV. Here, the conductivity for both the structures of CZTS and CZTSe has the highest value. Afterwards, it decreases with the energy; higher energy implies that the material does not interact with incident photon.

The absorption band edges of CZTS_KS, CZTS_SS, CZTSe_KS, and CZTSe_SS with scissor correction using GGA and TB-mBJ are shown in Fig. 7. The band gap energies (E_g) of CZTS and CZTSe were calculated from the Tauc's plot assuming $\alpha^2 \propto (h\upsilon - E_g)$, where α is the absorption coefficient and $h\upsilon$ is the photon energy (h is the Planck's constant and υ is the frequency). It is found that the theoretical absorption spectra of CZTS_KS and CZTSe_KS agree well with the available experimental spectra [1, 22, 28, 29] in their shape. The estimated band gaps using TB-mBJ including scissor correction are 1.58, 1.63, 1.34, and 1.55 eV for CZTS_KS, CZTS_SS, CZTSe_KS, and CZTSe_SS, respectively, (Fig. 7). All these values are quite close to the experimental value for a single-junction solar cell [28, 30–33]. The absorption coefficient was higher than 10^4 cm^{-1} in the visible region. Actually, the absorption coefficient, $\alpha(\omega)$ of CZTS_KS, CZTS_SS, CZTSe_KS, and CZTSe_SS represent the linear optical response from the valence bands to the lowest conducting bands. All three components have comparable absorption, although with different photon energies for the onset to absorption (i.e., the band gap energy). The absorption starts in the energy of fundamental gap. In the energy range of 1.1–1.8 eV, the absorption peaks are due to the transition of electron in the hybridized states of Cu-*d* and anion-*p* to empty states in the CB. The value of $\alpha(\omega)$ increases as the energy increases to its higher value. Therefore, it is worthy to investigate extensively CZTS and CZTSe for the sake of obtaining high-efficient materials.

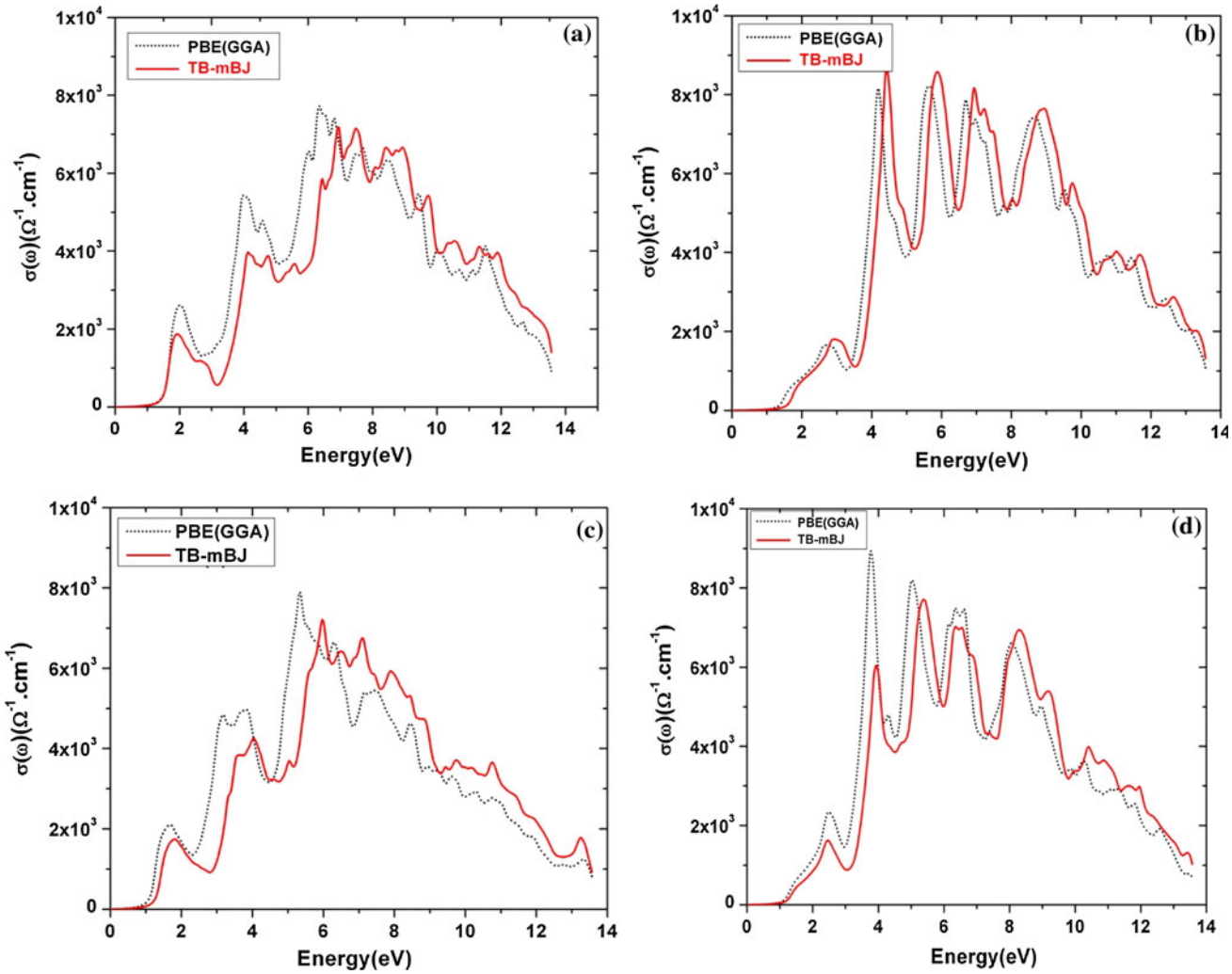

Fig. 6 (Colar online) **a–d** represent the calculated real part of the optical conductivity spectra of CZTS_KS, CZTS_SS, CZTSe_KS, and CZTSe_SS, respectively

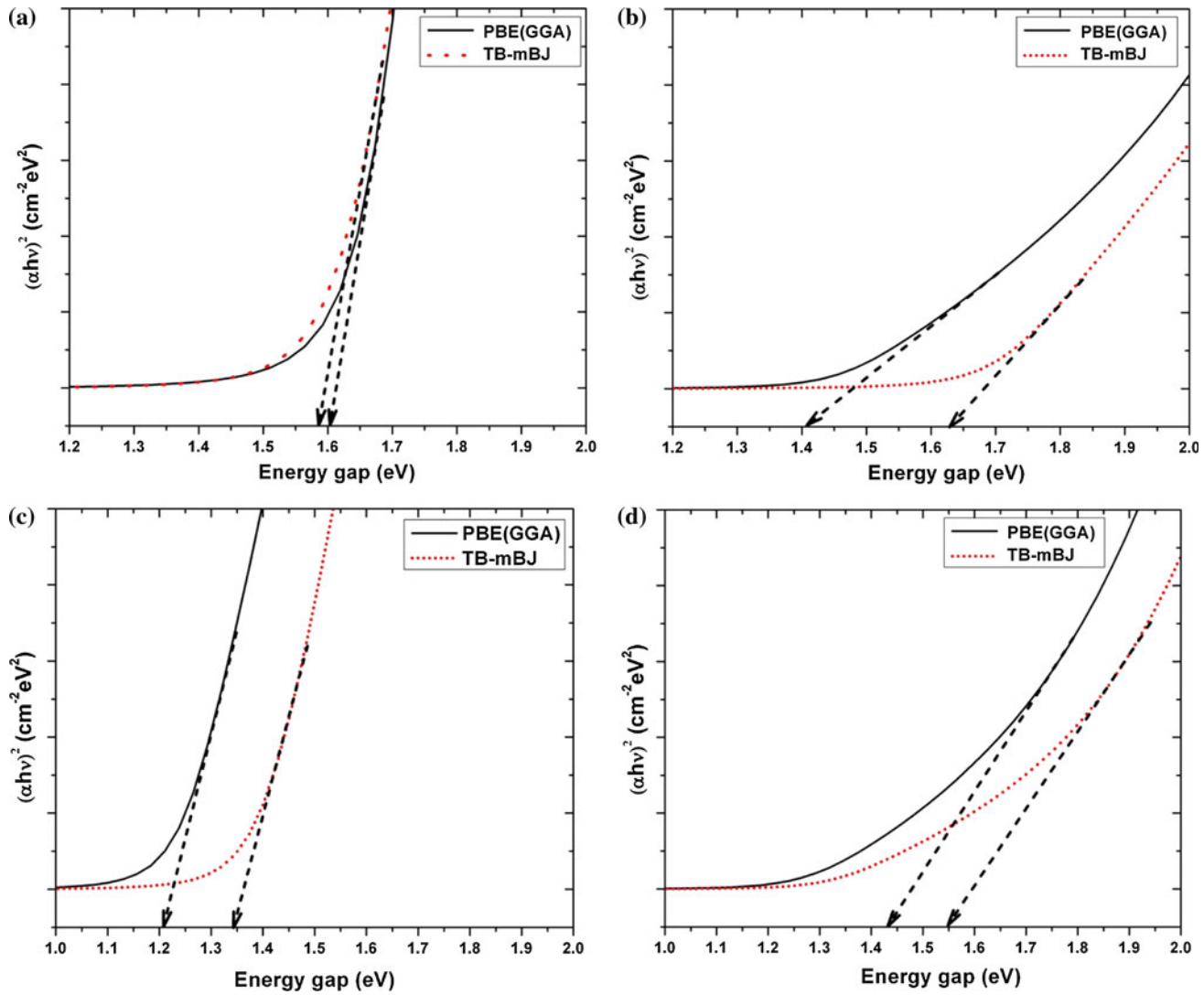

Fig. 7 (Color online) **a–d** represent the calculated $(\alpha h\upsilon)^2$ versus energy gap (eV) of CZTS_KS, CZTS_SS, CZTSe_KS, and CZTSe_SS, respectively

Conclusion

In summary, we have used TB-mBJ exchange potential implemented in WIEN2K (FP-LAPW) method to investigate the electronic and optical properties of Cu_2ZnSnX_4 (X = S, Se). The calculated results show that the energy gaps are substantially improved by TB-mBJ over GGA values toward experimental results and also we found that the compounds are direct band gap semiconductors. The behavior of optical dielectric functions (both real and imaginary parts) and optical conductivity and absorption coefficients as functions of photon energy agree well with the experimental and other literature values. The present study reveals that these excellent improvements are achieved because TB-mBJ potential describes accurately the hybridization between the Zn-*s* and anion (S and Se)-*p* states.

Acknowledgements The authors thank the Indian School of Mines, Dhanbad, India, for providing the Junior Research Fellowship.

References

1. Persson C (2010) J Appl Phys 107:053710
2. Suryawanshi MP, Agawane GL, Bhosale SM, Shin SW, Patil PS, Kim JH, Moholkar AV (2013) Mater Technol Adv Perform Mater 28:98
3. Walsh A, Chen Su, Wei S-H, Gong X-G (2012) Adv Energy Mater 2:400
4. Zhao Z, Chenshuo M, Cao Y, Juan Y, Xijia He, Qiu J (2013) Phys Lett A 77:417
5. Zhao H, Persson C (2011) Thin Solid Films 519:7508
6. Sevik C, Cagin T (2010) Phys Rev B 82:045202
7. Liu HR, Chen S, Zhai YT, Xiang HJ, Gong XG (2012) J Appl Phys 112:093717
8. Maeda T, Nakamura S, Wada T (2011) Jpn J Appl Phys 50:04DP07

9. Tran F, Blaha P (2009) Phys Rev Lett 102:226401
10. David K, Tran F, Blaha P (2012) Phys Rev B 85:155109
11. Shiyou C, Gong XG, Aron W, Wei S-H (2009) Appl Phys Lett 94:041903
12. Singh DJ (2010) Phys Rev B 82:155145
13. Singh DJ, Seo SSA, Lee HN (2010) Phys Rev B 82:180103
14. Blaha P, Schwarz K, Madsen GKH, Kvasnicka D, Luitz J (2001) WIEN2K an augmented plane wave + local orbitals program for calculating crystal properties, Karlheinz Schwarz, Techn. University at Wien, Austria ISBN 3-501031-1-2
15. Perdew JP, Burke K, Ernzerhof M (1996) Phys Rev Lett 77:386
16. Monkhorst HJ, Pack JD (1976) Phys Rev B 13:5188
17. Okoye CMI (2003) J Phys Condens Matter 15:5945
18. Amin B, Ahmad MI, Maqbool S, Said G, Ahmad R (2011) J Appl Phys 109:023109
19. Sun J, Wang H, He J, Tian Y (2005) Phys Rev B 71:125132
20. Ozaki S, Adachi S (1994) J Appl Phys 75:7470
21. Saha S, Sinha TP (2000) Phys Rev B 62:8828
22. Yakuphanoglu F (2011) Sol Energy 85:2518
23. Matsushita H, Maeda T, Katsui A, Takizawa T (2000) J Cryst Growth 208:416
24. Kamoun N, Bouzouita H, Rezig B (2007) Thin Solid Films 515:15
25. Katagiri H, Sasaguchi N, Hando S, Hoshino S, Ohashi J, Yokota T (1997) Sol Energy Mater Sol Cells 49:1
26. Zoppi G, Forbes I, Miles RW, Dale PJ, Scragg JJ, Peter LM (2009) Prog Photovolt 17:5
27. Joachim P, Ryoji A, Akihiro N, Georg K (2009) Phys Rev B 79:115126
28. Tanaka K, Oonuki M, Moritake N, Uchiki H (2009) Sol Energy Mater Sol Cells 93:583
29. Rajesh G, Muthukumarasamy N, Subramaniam EP, Agilan S, Velauthapillai D (2013) J Sol Gel Sci Technol. doi:10.1007/s10971-013-3006-9
30. Jiang M, Li Y, Dhakal R, Thapaliya P, Mastro M, Caldwell JD, Kub F, Yan X (2011) J Photonics Energy 1:019501
31. Katagiri H, Ihigaki N, Ishida T, Saito K (2001) Jpn J Appl Phys 40:500
32. Seol J, Lee S, Lee J, Nam H, Kim K (2003) Sol Energy Mater Sol Cells 75:155
33. Zhao Z, Chenshuo M, Yuechan C, Juan Y, Xijia H, Jianbei Q (2013) Phys Lett A 377:417
34. Todorov TK, Reuter KB, Mitzi DB (2010) Adv Mater 22:20
35. Oliveira TA, Coutinho J, Torres VJB (2013) Thin solid films 535:311
36. Babu GS, Kumar YBK, Bhaskar PU, Raja VS (2008) Semicond Sci Technol 23:8